

# Shake Table Test of Structure Reinforced with Superelastic Dampers

**M. Branco & L. Guerreiro**

*ICIST, Instituto Superior Técnico, Universidade Técnica de Lisboa*

**A. Campos Costa & P. Candeias**

*LNEC, Laboratório Nacional de Engenharia Civil*



## SUMMARY:

The energy dissipation capacity of the NiTi alloy was evaluated as part of a series of shake table tests. A superelastic damper was developed to take advantage of the hysteretic energy dissipation associated with this type of shape memory alloy. Each device was tested at different intensity levels with 4 NiTi wires, all with 0.9mm of diameter. A steel cantilever with 600 kg mass on top was subjected to a series of ground motions with different intensities. The dampers were placed as part of a tie system, restraining the movement of the top mass. The devices showed stable hysteretic behaviour allowing for a reduction in relative displacement as well as energy dissipation. An equivalent hysteretic damping ratio around 20% was obtained with the use of the superelastic dampers.

*Keywords: Superelastic damper; shape memory alloy; shake table test; energy dissipation.*

## 1. INTRODUCTION

The superelastic damper (SD) presented in this work takes advantage of the energy dissipation associated to the mechanical deformation of shape memory alloys (SMAs). SMAs belong to a group of materials known as smart materials, having the possibility to recover from large strain deformation through cycles of stress or temperature. The ability to recover from considerable deformation is associated to a diffusionless transformation in the alloys crystalline mesh, without variation of its chemical composition, designated as martensitic transformation. The SMA, when subjected to stress or cooling, transforms from austenite, which is stable at higher temperatures, to martensite, stable at lower temperatures. The ability to recover the original shape through stress induced cycles is designated as superelastic effect (SE). If the martensitic transformation is associated to temperature cycling then it is designated as shape memory effect (SME). Both are schematically exemplified in Figure 1 [Otsuka and Wayman (1998), Lagoudas (2008)].

The superelastic property, which is the basis of the device developed in this study, allows recovering from considerable stress induced deformation (up to 8% strain), without significant residual elongation. Additionally, when the phase transformation is undergone, a considerable reduction in stiffness is observed until the material reaches the full martensitic configuration, after which there is an increase in stiffness. When unloaded the material recovers the original undeformed shape, but the transformation occurs for a lower stress plateau, which causes energy to dissipate due to a hysteretic phenomenon (Figure 1) [Otsuka and Wayman (1998), Lagoudas (2008)].

There are already several prototypes developed that combine the energy dissipation to re-centering capacity. For example, Ma and Cho (2008) developed a damper composed by pre-stressed NiTi wires and two NiTi pre-compressed springs, which work to dissipate energy and re-center respectively. Aiken and Kelly (1990) tested a bracing system, which increased the damping in a structure from 0.5% to 3%, with reduction of the remaining structural responses. Another series of tests performed by Dolce and co-workers intended to evaluate different devices for bracing structures with and without

re-centering behavior. For each test, different alloys, diameter and number of wires and pre-strain level were evaluated. The dissipation mechanism was tested with both martensitic bars and pre-strained austenitic wires [Cardone et al (1999), Coelho et al (2000), Dolce and Maranetto (1999)].

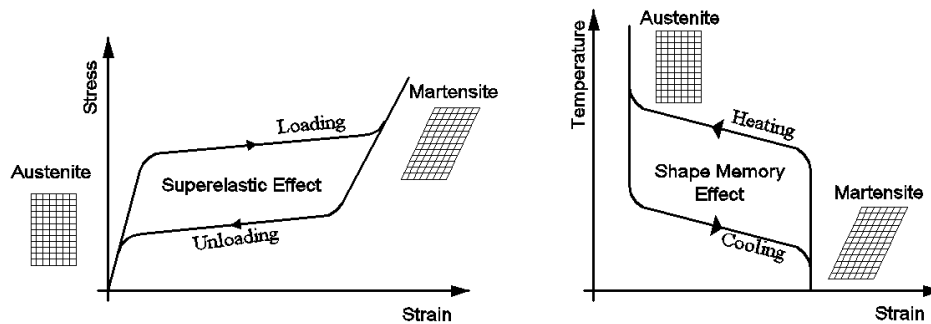


**Figure 1.** Martensitic transformation: left – superelastic effect; right – shape memory effect.

First of all by concentrating the energy dissipation and re-centering capacity in one material, a simple and clean device is obtained. Furthermore the behavior of the SMA, in the present case NiTi, shows very stable behavior for the range of frequencies of vibration expected during the event of an earthquake [Cardone et al (1999)]. In this paper the superelastic property is used to increase the energy dissipation of a steel cantilever subjected to different levels of ground motion excitation.

## 2. MATERIALS AND EXPERIMENTAL SETUP

### 2.1. Superelastic damper

The SD was designed to take advantage of the superelastic behavior of NiTi wires and convert them into part of earthquake protection system. Therefore, the device has to allow for a good cyclic behavior, with the possibility to apply pre-strain and work only in tension. When compared to previous solutions presented, this system is intended for experimental validation, although its working principle can be adapted for practical applications with some modifications.

This device was composed of several steel plates which work as a link between the NiTi wires and a steel rope. In Figure 2 the device is presented. One of the plates is welded to two lateral plates, while the other one slides along two slots on the lateral plates. The wires should be placed when the main plates are in the closest configuration, so they work only in tension. This way, in case of compression the lateral steel plates would work as battens and block any movement.

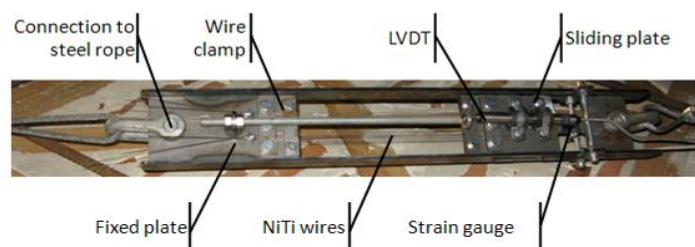


**Figure 2.** Superelastic damper.

In order to record essential data regarding axial force and displacement on the NiTi wires, the sliding plate had a section reduced, in order to increase the strain so it could be measured with strain gauges, installed in a full bridge configuration. In addition, a support for a linear variable differential transformer (LVDT) was added so the displacement between each plate could be measured and the wires strain could be determined (Figure 2). For these tests, four SD devices were used with 0.889 mm diameter NiTi wires. The device was tested with 4 wires.

## 2.2. Experimental setup

The present tests were performed at Núcleo de Engenharia Sísmica e Dinâmica de Estruturas (NES-DE) at Laboratório Nacional de Engenharia Civil (LNEC) at the shake table LNEC-3G [Bairrao and Vaz (2000)]. For this test, a mass on top of a steel cantilever was subjected to a series of ground excitations. Two masses with 600 kg were used, one was placed on top of a HEB100 profile to be excited and the other was placed at the base to ensure the connection between the profile and the shake table, totaling a height of 2.85 m. This structure was placed in the center of the shake table and it was connected to four ties containing the SDs. Each tie had a total length of approximately 3.4 m, which was divided amongst the SD, one forged straining screw and steel wire rope. The rope selected for this series of tests has 8 mm diameter and a modulus of elasticity of 125 GPa. The main requirement for the steel cable was that its elongation would be negligible when compared with the elongation of the NiTi wires.

The forged straining screw was used to apply a pre-strain to the NiTi wires, so they would work in the tensile transformation area. A schematic view of the experimental setup is presented in Figure 3, where each SD is numbered. The profile was oriented with the web parallel to the longitudinal axis of the shake table (stronger direction, x) and the flanges parallel to the transversal axis (weaker direction, y) (Figure 3 a).

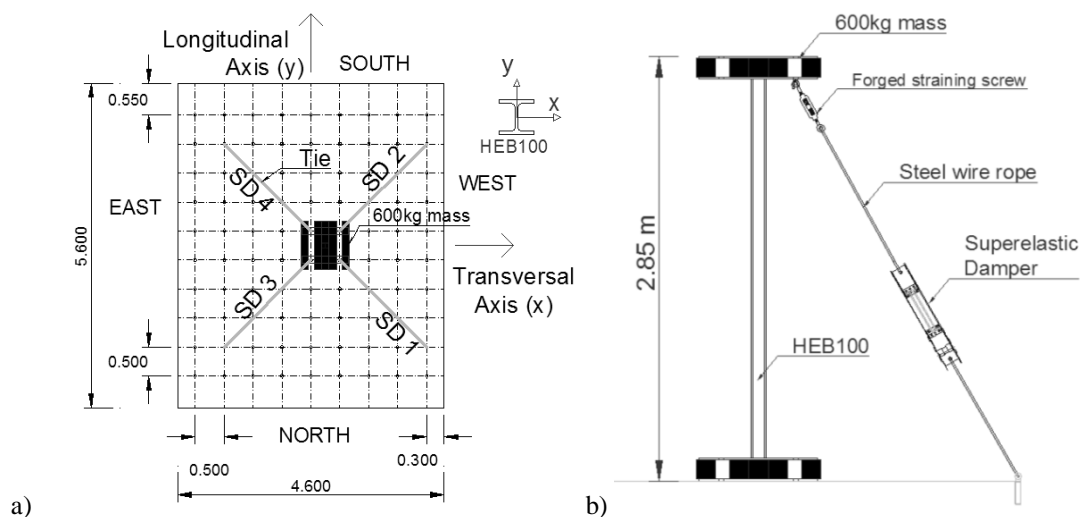


**Figure 3.** Scheme of the assembly for the shake table test: a) plan view; b) lateral view.

Two sets of accelerometers were installed in two different extremities on top of the mass, to measure the acceleration along three orthogonal axis and to detect any movement associated with torsion of the profile. Two additional accelerometers were placed at the base of the structure measuring horizontal orthogonal accelerations. The dynamic measuring system Krypton K600 was used to record the three dimensional displacement of the structure at different points. Twelve LEDs were placed along the height of the profile. An extra LED was placed at the base of the structure in order to measure the ground displacement.

The structure was tested with and without the restraining ties for different artificial ground motions, applied to both orthogonal horizontal directions simultaneously. Instead of using recorded ground motions from actual earthquakes, it was considered more relevant to use signals with a high energy content along a significant band of frequencies. This way a more accurate dynamic characterization of the structure and dampers would be achieved. In any phase of this series of tests, no vertical ground motion was considered. Four pairs of time-histories with increasing level of spectral acceleration, up to 400% the lowest intensity ground motion were adopted.

### 3. RESULTS AND DISCUSSION

An initial pre-strain was applied to ensure that the deformation of the NiTi wires would concentrate in the superelastic range and that they would work always in tension. The pre-strain was applied by manually tightening the forged straining screws. During this procedure the deformation and axial force in the wires was monitored so they would have approximately the same initial conditions in the beginning of the shake table test. As manual tightening was done, some variation between devices was acceptable. Furthermore, as the transformation plateaus are almost horizontal a deviation in strain does not lead to significant variation in stress. At the start of the dynamic tests, the wires were subjected to a pre-strain around 0.04, which is the middle of the superelastic range, corresponding to a stress of approximately 400 MPa per NiTi wire.

#### 3.1. Modal analysis

##### 3.1.1. Unrestrained structure

A preliminary test was conducted to the unrestrained structure in order to perform its modal characterization. To this purpose the structure without the SDs was subjected to the ground motions as previously characterized, in both orthogonal horizontal directions.

For the modal characterization of the unrestrained structure, the frequency response function (FRF) was determined as a function of the relation between the output and the input power spectra. The result is a complex function, which is characterized by magnitude (measured in dB) and phase (measured in rad), as presented in Figure 4, for each direction and the 100% ground motion.

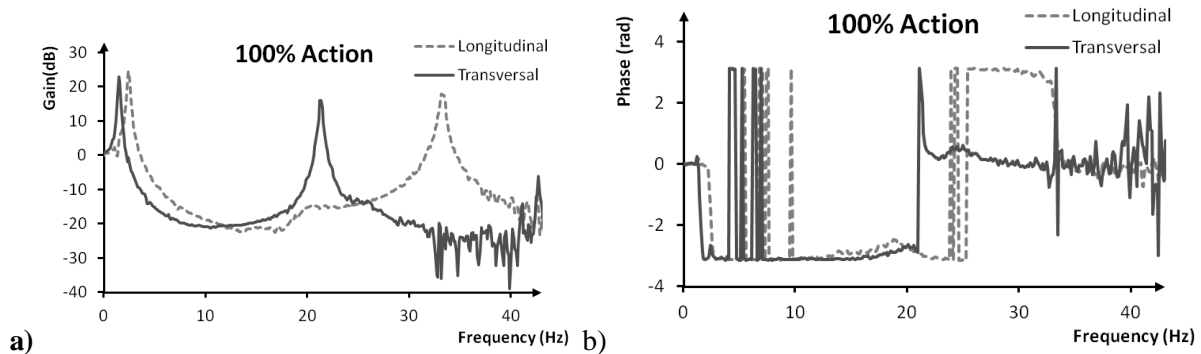


**Figure 4.** FRF between base acceleration and top acceleration for the unrestrained structure for 100% ground motion of set 3: a) magnitude; b) phase.

From the definition of the FRF, the frequencies of vibration of the principal modes could be determined through the method of peak amplitude [Proença (1989), Proença and Azevedo (1999)]. Through the observation of Figure 4 a), the most evident peaks yielded a frequency of vibration of 1.51 Hz for the transversal direction and 2.40 Hz for the longitudinal direction. A second mode of vibration was also detected in both directions at 21.24 Hz for the transversal direction and 33.20 Hz for the longitudinal direction.

The damping ratio ( $\xi$ ) of the structure was determined through the half power method. Using this method, an increase in damping is observed with the increase in the intensity of the ground motion. Also the transversal direction presents a higher damping coefficient than the longitudinal direction, possibly as an effect of the clamping system in the base. The damping ratio was calculated in the range of 3.3% to 5.2%.

##### 3.1.2. Structure with SDs

With the introduction of the ties incorporating the SD, the modal characteristics of the system were modified due to changes in stiffness. Therefore, the frequencies of vibration for this setup were also

computed and compared to the previous results.

The magnitude of the FRF is presented in the following figure for the 100% and 400% ground motion (Figure 5) for the structure with SDs. In contrast with the unrestrained structure, both directions show similar results for the first mode of vibration. A first peak appears around 2.4 Hz in both directions and a new peak appears in the range of 3 to 4 Hz. At a significantly higher frequency another mode of vibration is identified above 20 Hz as it had already been noticed in the unrestrained structure. Nevertheless, the two low frequencies tend to merge as the ground motion intensity increased. The lowest frequency of vibration is assumed to be associated to the vibration of the steel ties.

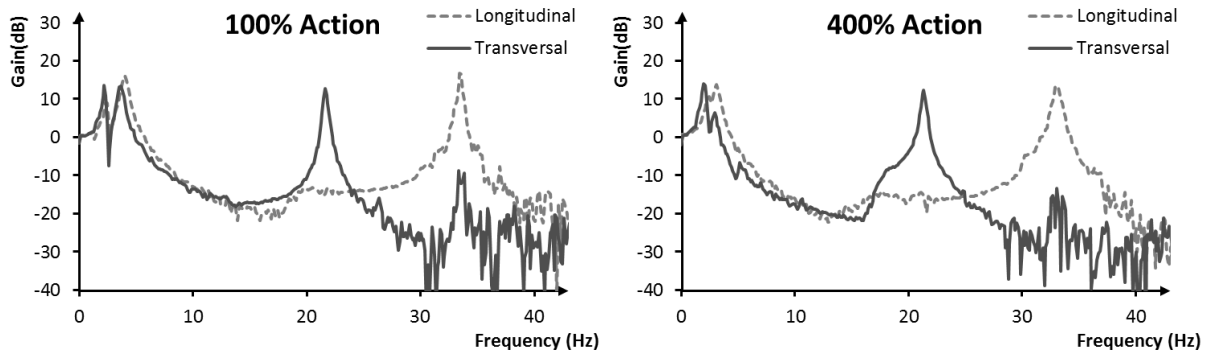


**Figure 5:** FRF for SD for the 100% and 400% ground motion.

As observed in Table 3.1, a slight reduction in frequencies of vibration was observed with the increase of the intensity of the ground motion. For the first mode of vibration a reduction from 2.20 Hz to 1.83 Hz was recorded, from the 100% ground motion to the 400% ground motion. A similar reduction is observed for the second mode of vibration. This could be associated to a reduction in stiffness as a result of the shape of the hysteretic loops of the NiTi alloy.

**Table 3.1.** Frequencies of vibration for structure with SDs.

	100%		200%		300%		400%	
	Long.	Transv.	Long.	Transv.	Long.	Transv.	Long.	Transv.
<b>1st Mode</b>	2.31	2.20	2.19	2.07	2.31	1.95	2.31	1.83
<b>2nd Mode</b>	3.90	3.40	3.54	3.17	3.17	2.32	2.92	2.31
<b>3rd Mode</b>	33.32	21.6	33.2	21.48	33.08	21.36	32.83	21.24

### 3.3. Structural response

A structure subjected to ground excitation mobilizes three main forces which related through the well-known equation of motion: the inertia force ( $f_i$ ) associated to the acceleration of the mass in motion, the damping force associated to viscous behavior of the material ( $f_D$ ) and finally the restoring force ( $f_s$ ) associated to the deformation of the structure. This last component is divided into an elastic part which is recovered after deformation and an inelastic part which is not recovered and it is associated to energy dissipation through hysteretic phenomena.

The inertia force was determined by the second law of motion, only considering the inertial effect of the lumped mass ( $m$ ) of 600 kg on top of the structure. In this particular case, the restoring force is computed as the sum of the total base shear, which is the sum of the shear in the steel cantilever ( $V(t)$ ) and the horizontal component of the axial force of each tie ( $N_h(t)$ ). The damping force is the result of the multiplication of a damping coefficient ( $c$ ) and the relative velocity of the mass ( $\dot{u}_r(t)$ ). As the definition of the damping coefficient is not straightforward, an indirect approach was adopted as the symmetric of the sum of the inertia and restoring forces.

When analyzing the performance of a damper for seismic protection, the use of energy as one of the

main criteria is common. By integrating each parameter of the equation of motion in order to the relative displacement ( $u_r$ ), the energy equation is determined [Uang and Bertero (1988)]. The total energy introduced in the system is composed by the absorbed energy by the system ( $E_a$ ) associated to the hysteretic behavior, the damped energy ( $E_d$ ) which is associated to the energy dissipated through viscous phenomena and the kinetic energy ( $E_k$ ) [Uang and Bertero (1988)]. This work will focus specially in the evaluation of the absorbed energy, as it is associated to the hysteretic behavior of the superelastic damper.

In order to have a basis of comparison, the unrestrained structure was also subjected to the same ground motion as the reinforced structure. As an example of the improvement of the structural behavior with the implementation of the SD, in Figure 6 and Figure 7 the relative displacement of the top mass is shown in time for the unrestrained structure and for the structure with SDs for the 400% ground motion. A significant reduction in the displacement is observed in both directions.

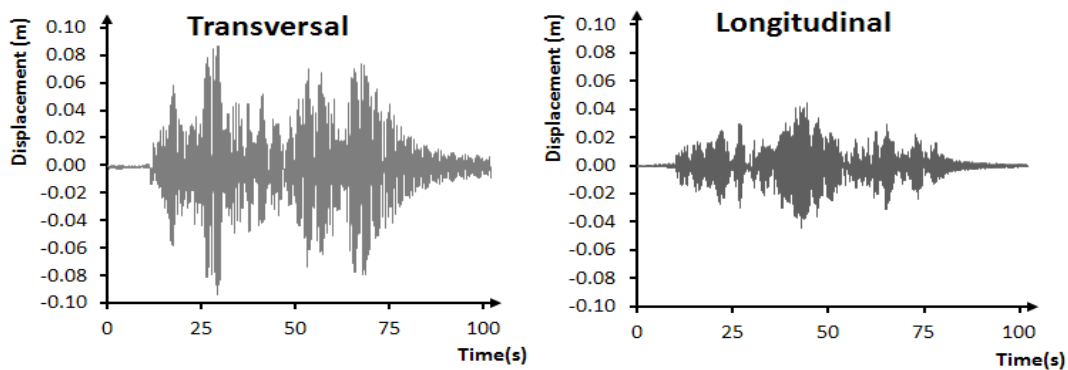


Figure 6. Relative displacement for unrestrained structure for 400% ground motion.

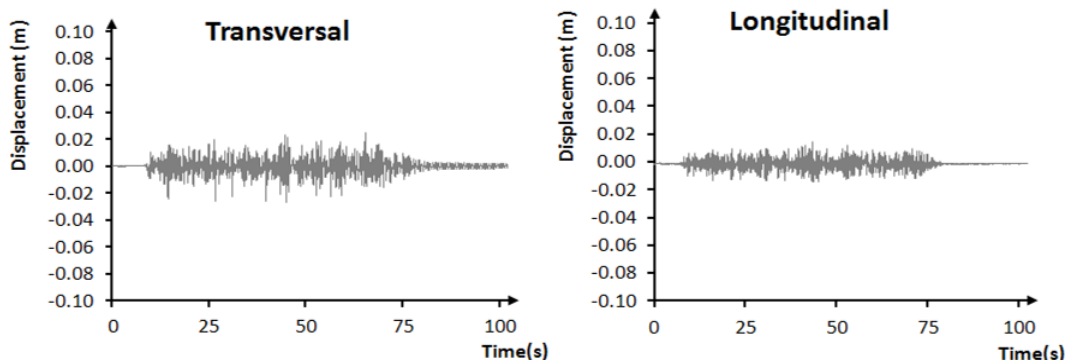


Figure 7. Relative displacement for stage 4 tests for 400% ground motion.

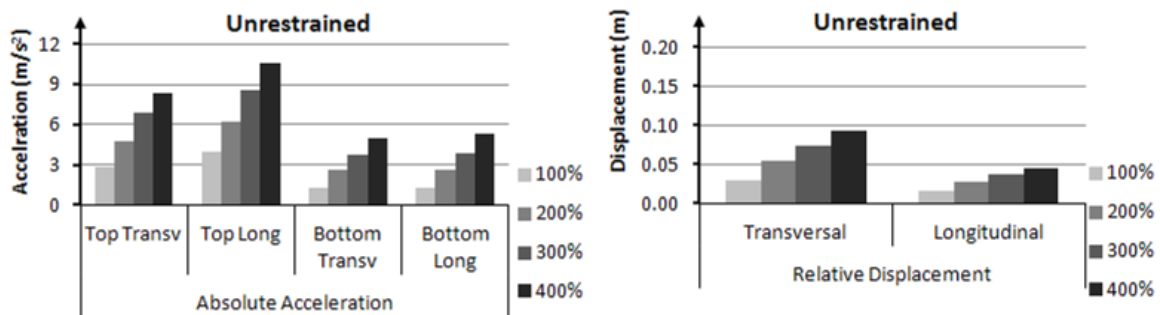


Figure 8. Maximum acceleration and displacement for unrestrained structure.

A more complete analysis is given by the observation of Figure 8 and Figure 9 where the maximum

absolute and relative accelerations and displacements are shown for both horizontal directions for the unrestrained structure and after the implementation of the SDs. Regarding to relative displacements, significant reduction was also observed with the introduction of the SDs. Besides the reduction in displacement the use of ties produced a similar dynamic response in both directions, as opposed to the unrestrained structure which has a higher response along the transversal direction. This comes as a result of the increase in stiffness introduced the ties, which compensate the difference in stiffness along the strong and weak axis of the profile.

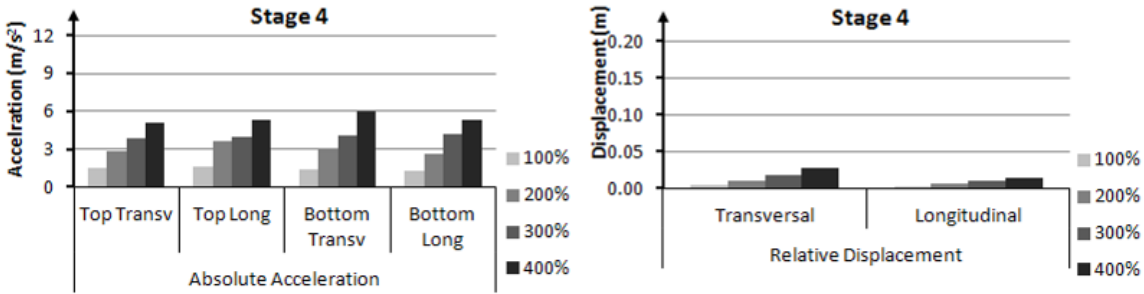


Figure 9. Maximum acceleration and displacement for structure with SDs.

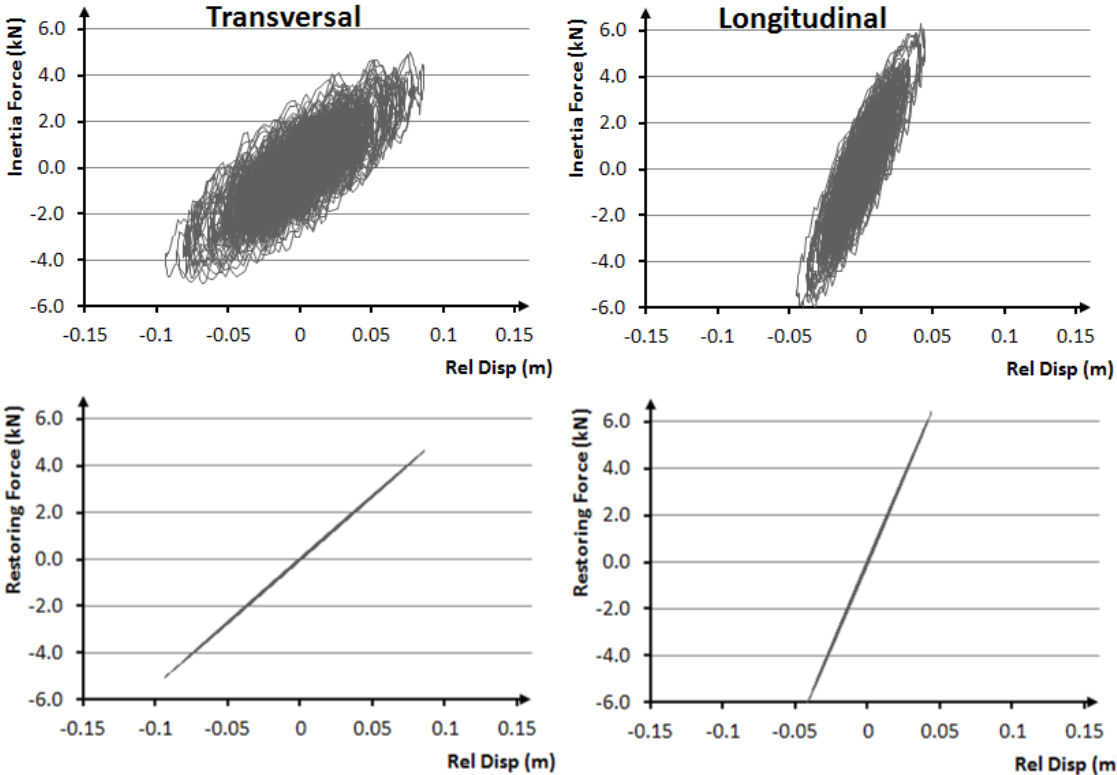
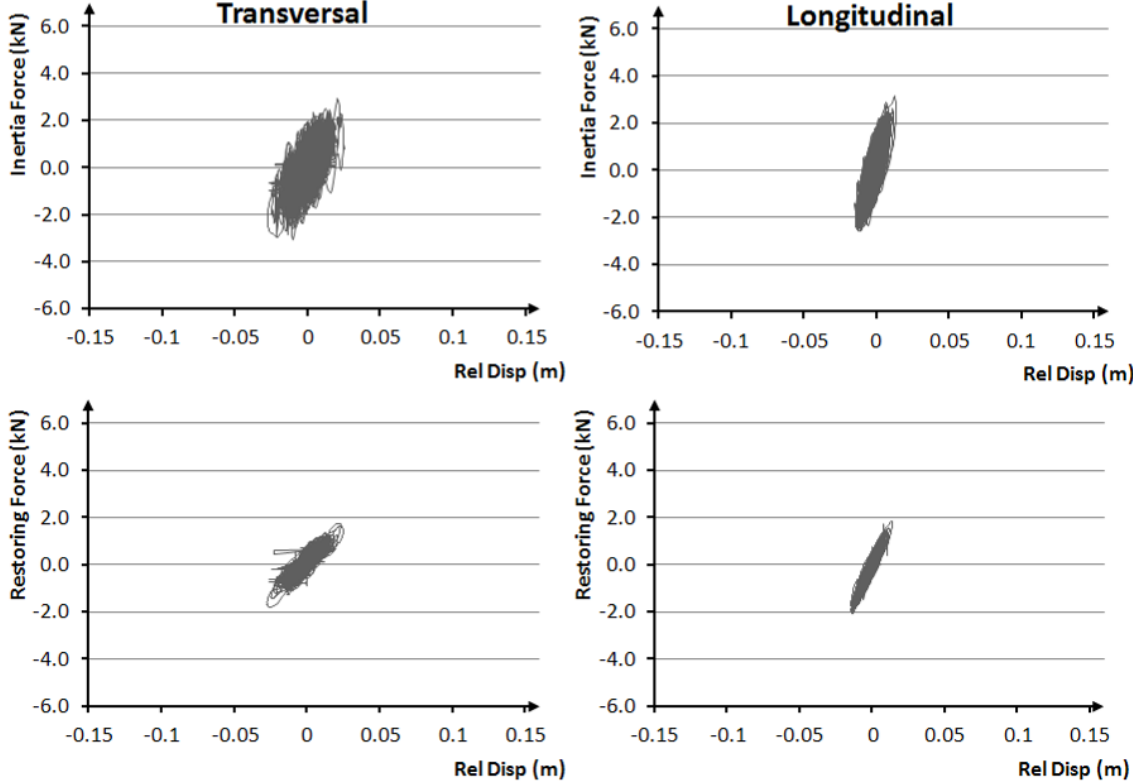


Figure 10. Inertia force, restoring force and damping force for the unrestrained cantilever subjected to the 400% ground motion of set 3 along the transversal (left) and longitudinal (right) directions.

In Figure 10 and Figure 11 the force/displacement diagrams for the inertia force and restoring force were presented for the case with and without the SDs for the 400% ground motion. Although the ranges differ from one case to the other, the diagrams presented similar patterns for the inertia and damping forces. The most significant difference was noticed for the restoring forces. While for the unrestrained structure a linear response was observed, with the introduction of the SDs a more elliptical diagram was obtained indicative of inelastic behavior associated to the hysteretic behavior of the NiTi wires.

From the restoring force diagram, the energy dissipated along the experiment could be determined through integration. The results are presented in Figure 12 for both directions. An overall increase in energy dissipation is reported in time until a maximum value. The results show higher energy dissipation along the longitudinal direction with 0.97 kJ against 0.88 kJ along the transversal direction for the 400% ground motion.



**Figure 11.** Inertia force and restoring force for stage 4 tests subjected to the 400% ground motion along the transversal (left) and longitudinal (right) directions.

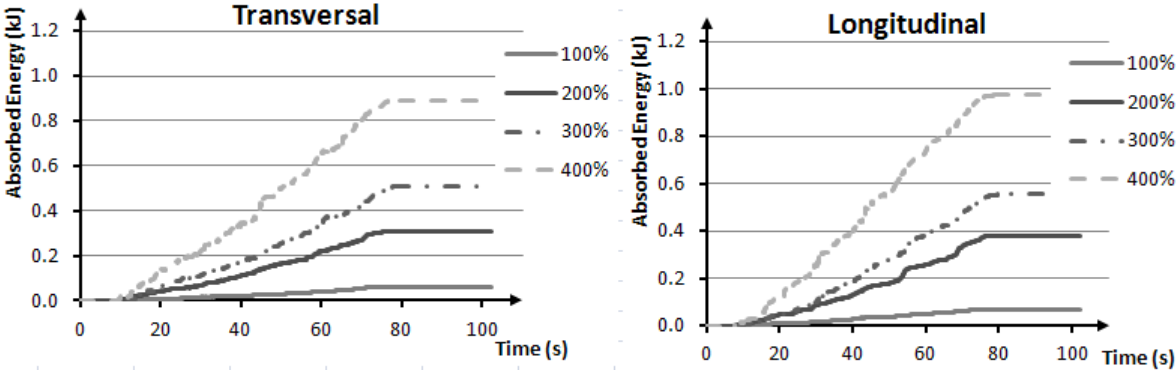


**Figure 12.** Absorbed energy during stage 4 of tests.

After analyzing the global performance of the structure it was also important to analyze the performance of the superelastic dampers in detail. In Figure 13 the stress-strain diagrams for SD1 were shown for each level of ground motion. From the analysis of Figure 13 an increase in the area of the hysteretic loops was reported, growing from an almost linear behavior at 100% to a significant area at 400%. The behavior observed was closely adjusted to the preliminary dynamic tests done to characterize individual wires (dashed line).

By integrating the stress-strain diagram, the specific energy dissipated per unit of volume of NiTi

could be calculated and was presented in Figure 14. In this stage, the results from the four dampers were very similar with an average maximum energy dissipation of  $505 \text{ MJ/m}^3$ . In Figure 14, the energy dissipated for the different levels of ground motion intensity was presented. The energy dissipation shows very similar results between each one of the dampers, for all the ground motions tested. In one hand this gives information on the reliability of these devices and the possibility of replicating results.

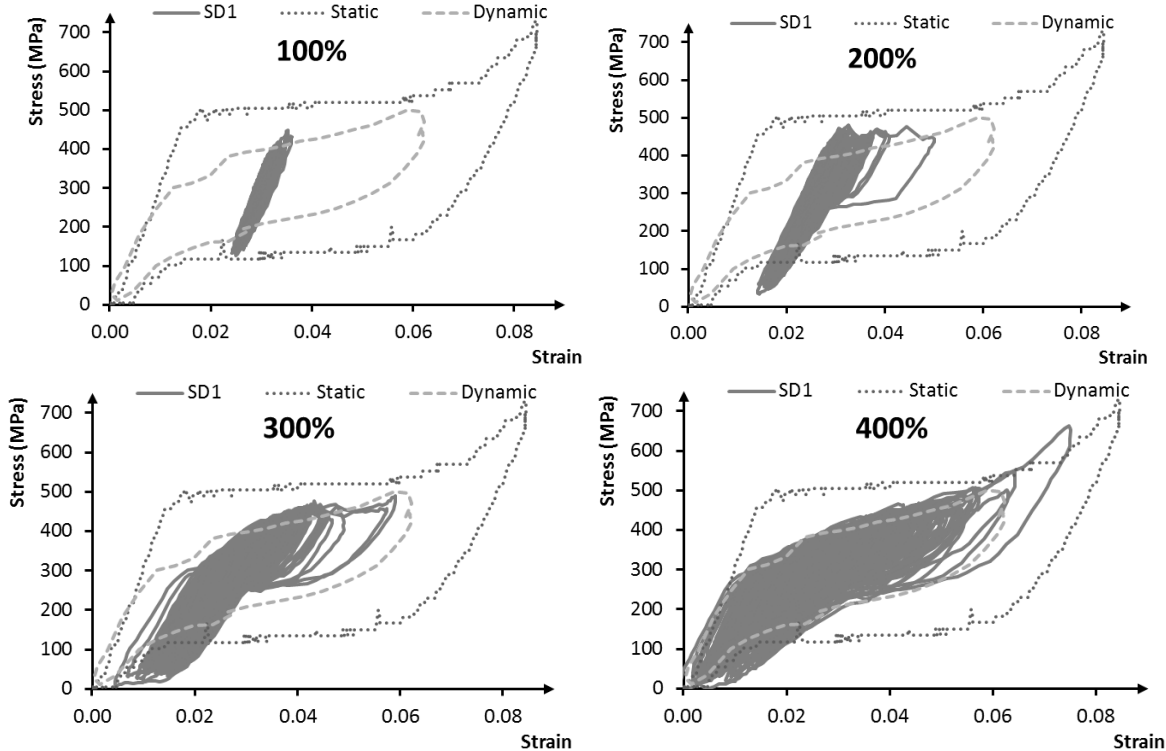


Figure 13. Stress-strain diagram for SD1 in stage 4 of tests.

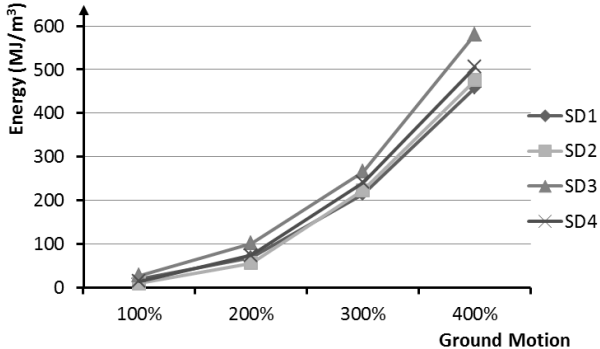


Figure 14. Energy dissipated per volume of NiTi wire in each SD during stage 4.

4. CONCLUSIONS

A series of shake table tests were performed to evaluate the performance of a superelastic damper, that takes advantage of the hysteretic behavior associated to mechanical loading of NiTi wires. To properly characterize the dynamic behavior of this device a simple structure consisting of a mass on top of a cantilever was subjected to different series of ground motions. The SDs were implemented as part of ties that restrained the movement of the top pass and dissipated energy.

A significant reduction in displacement and acceleration was observed for every setup tested, when compared to the unrestrained structure. The energy dissipation determined from the restoring

force/displacement diagram evidenced a steady increase with the increase in load intensity.

When analyzing the performance of each device independently, a significant level of energy dissipation is observed. Furthermore, the stress-strain diagrams for each SD presented consistent results and good ability to replicate the single wire tensile tests performed during the material characterization.

Overall the results obtained from this series of tests assessed on the energy dissipation capacity of NiTi wires and its ability to be used as part of superelastic dampers. Also the devices demonstrated good cyclic behavior and replication of results. These conclusions allow the basis for further research for the development of superelastic dampers that could be implemented as part of earthquake strengthening designs.

#### **ACKNOWLEDGEMENT**

This research is financially supported by the Foundation for Science and Technology of Portugal (Fundação para a Ciência e Tecnologia) under grant number SFRH / BD / 43539 / 2008. This work was made in cooperation between the Instituto Superior Técnico and the Laboratório Nacional de Engenharia Civil. We acknowledge the support of all these institutions and the laboratory staff that supported this experimental campaign. Particularly we acknowledge the help of Mr. Fernando Alves in manufacturing the devices and the work and the support from Mr. Artur Santos, Mr. Gonçalo Vitor and Mr. Miguel in the setup of the experiment. We further acknowledge the help of the Núcleo de Sistemas Electrotécnicos, directed by Eng. Almeida Garret in the setup of the strain gauges.

#### **REFERENCES**

- Otsuka, K. and Wayman, C.M. (1998) Shape Memory Materials. Cambridge : Cambridge University Press.
- Lagoudas, D. (2008) Shape Memory Alloys – Modeling and Engineering Applications. New York : Springer.
- Ma, H. and Cho, C. (2008) Feasibility study on a superelastic sma damper with re-centring capability. Materials Science and Engineering A., Vol. 473, pp. 290–296.
- Aiken, I. D. and Kelly, J. M. (1990) Earthquake simulator testing and analytical studies of two energy- absorbing systems for multistory structures. s.l. : University of California, Berkeley Report UCB/EERC-90-03.
- Cardone, D., Dolce, M. and Nigro, D. (1999) Experimental Tests on SMA based Seismic Devices. Memory Alloys for New Seismic Isolation and Energy Dissipation Devices, Workshop Proceedings January 28-29. Rome : s.n..
- Coelho, E., et al. (2000) Comportamento sísmico experimental de estruturas de betão armado reforçadas com dispositivos dissipadores de energia. REPAR 2000. Lisboa : LNEC.
- Dolce, M. and Marnetto, R. (1999) Seismic Devices based on Shape memory alloy – Manside Project. Rome : Italian Department for National Technical Services.
- Bairrao, R. and Vaz, C.T. (2000) Shaking table testing of civil engineering structures - the LNEC 3D simulator experience. Proceedings 12WCEE 2000: World Conference on Earthquake Engineering.
- Proença, J.M. (1989) Identificação Dinâmica de Sistemas Estruturais. Técnicas Experimentais e Analíticas - Thesis for the degree of Master in Structural Engineer. Lisbon : IST.
- Proença, J.M. and Azevedo, J. (1999) Identificação Dinâmica de Sistemas Estruturais - Conceitos Gerais - Disciplina de Dinâmica de Estruturas. Lisbon : IST.
- Uang, C.M. and Bertero, V.V. (1988) Use of energy as a design criterion in earthquake-resistant design. Berkeley : Earthquake Engineering Research Center.